IEEE Access
Multidisciplinary | Rapid Review | Open Access Journal

Received January 4, 2019, accepted January 17, 2019, date of publication January 25, 2019, date of current version February 12, 2019.

Digital Object Identifier 10.1109/ACCESS.2019.2895053

Adaptive Neural-Based Finite-Time Trajectory Tracking Control for Underactuated Marine Surface Vessels With Position Error Constraint

MINGYU FU, TAIQI WANG, AND CHENGLONG WANG
College of Automation, Harbin Engineering University, Harbin 150001, China
Corresponding author: Taiqi Wang (wangtaiqi@hrbeu.edu.cn)

This work was supported by the National Natural Science Foundation of China under Grant 51309062.

ABSTRACT This paper addresses the trajectory tracking control problem of an underactuated marine surface vessel with position error constraint, finite-time convergence requirement, model uncertainties, and external disturbances. A barrier Lyapunov function is incorporated with the backstepping control scheme to handle the position error constraint. The command filters and auxiliary systems are designed to avoid the tedious analytical computation of the virtual control laws. Furthermore, an adaptive radial basis function neural network is adopted to provide the estimation of the unknown hydrodynamic damping term, and a disturbance observer is designed to compensate for the lumped disturbances including the neural approximation errors and external ocean disturbances. We show that under the proposed control scheme, the tracking errors of the vessel can converge to a small neighborhood around 0 within finite time, while the constraint on the vessel position is never violated during the maneuver, and all closed-loop signals are proved to be bounded. Finally, a numerical simulation is provided to illustrate the effectiveness and superiority of the proposed control scheme.

INDEX TERMS Marine surface vessel, finite-time control, trajectory tracking, barrier Lyapunov function.

I. INTRODUCTION

Due to the increasing exploitation of marine resources such as oil development, resources prospecting and transportations, the control problem of the underactuated marine surface vessel (MSV) has attracted considerable attention from the control community in the past few years [1], [2]. As one of the typical motion control scenarios for a MSV, trajectory tracking control, which forces a vessel to track the desired time-referenced trajectory, plays an important role in accomplishing these complicated tasks. However, the control design for an underactuated MSV encounters a serious challenge because the actuators are only equipped for surge and yaw motions, which implies that the independent control inputs are less than the degree-of-freedom (DOF) and leads to the non-integrable acceleration constraints on the sway dynamics [3]. In addition, the MSVs usually carry out the missions in the complex marine environment such that the dynamics of a MSV inevitably suffer from the perturbations including hydrodynamic coefficients and external marine disturbances induced by winds, waves and ocean currents [4]. Some control schemes [5], [6] have been proposed to solve the tracking control problem for MSVs. However, the model information is required to be completely known in the above papers, which hinders the adoption of these controllers in practice. Therefore, it is highly desirable to design robust tracking controllers for MSV control systems.

A number of control algorithms have been investigated for the trajectory tracking control of the disturbed MSV system. Sliding mode control (SMC) was adopted in [7]–[9] to develop the robust tracking controllers for underactuated MSVs, and the simulation results showed that good robustness can be obtained by employing there controllers. However, the discontinuous control signals in the above designs can result in the inherent chattering phenomenon on the rudders, which is harmful to the drive mechanism of a MSV. Subsequently, to overcome the drawback of input chattering, Sun *et al.* [10] and Xu *et al.* [11] introduced a continuous adaptive term to the SMC-based tracking con-

troller, and simulation results showed that the designed continuous sliding manifold can reduce the chattering of the input signals. Besides, the approximation-based control methods can also attenuate the effects of uncertainties. In such technique, the unknown vessel dynamics are identified by using appropriate neural networks (NNs) [12]–[14] or fuzzy logic systems (FLS) [15], [16], etc. In [17], the strong approximation capacity of neural network was integrated with backstepping control to design an adaptive robust tracking controller for an underactuated vessel, and the vessel can track the desired trajectory with good robust performance. Elhaki and Shojaei [18] presented a multi-layer neural network-based tracking controller to solve the target tracking problem by using neural adaptive control and prescribed performance control. Wang and Er [19] proposed an online self-constructing fuzzy neural approximator for a fully actuated vessel to achieve accurate estimation of uncertainties. However, it should be emphasized that the aforementioned control schemes can only ensure the asymptotic or exponential convergence of the tracking errors, which means that the settling time can be infinite in theory.

Note that finite-time control has been regarded as a powerful method to enhance convergence rate, tracking accuracy and disturbance suppression ability of a control system [20], [21]. As such, based on some control methods such as SMC [22], homogeneous technique [23] and adding a power integrator method (API) [24], the finite-time control-based tracking controller was extensively studied for the vessels to achieve faster tracking error stabilization. In [25], to achieve accurate trajectory tracking for MSVs, a finite-time robust tracking controller was proposed based on non-singular terminal SMC. In [26], an exact trajectory tracking controller was proposed for a fully actuated vessel, and the finite-time stability was guaranteed by combining homogeneous analysis and Lyapunov synthesis. In [27], a continuous finite-time tracking control scheme was obtained by virtue of API method for a fully actuated vessel with unknown disturbances. However, one important issue, the output constraint, was not considered in the aforementioned papers. The output constraints are of great importance to ensure navigation safety of a vessel. For example, the constraints on the position tracking error can make the actual route of a vessel remain in the prescribed range of the desired trajectory. It has been proved that barrier Lyapunov function (BLF)-based control is an effective solution to prevent the violation of constraint [28], [29]. In [15], [30], and [31], the output constraints of the fully actuated vessels were handled by using BLF-based adaptive control. However, only the asymptotic tracking is guaranteed and the control strategies for fully actuated vessels can not be directly applied for underactuated ones. Therefore, a novel finite-time tracking controller for a class of output-constrained nonlinear systems was proposed in [32] by utilizing a tan-type BLF. Jin [33] adopted the tan-type BLF to ensure the line-of-sight range and angle tracking errors constraints, while the formation tracking errors of the underactuated vessels can be stabilized in finite-time. Li *et al.* [34] designed a logarithm BLF-based controller to dispose full state constraints problem, and the tracking errors can be stabilized within finite time. However, the problem of trajectory tracking control for underactuated MSVs in the presence of unknown disturbances, position error constraints, and the finite-time convergence requirement, is still an open and challenging issue that has not been well addressed.

Motivated by the above observations, we present a novel finite-time trajectory tracking control scheme for an underactuated MSV with position error constraint and system uncertainties. In particular, the unknown hydrodynamic structure is estimated by using RBFNN, and the neural approximation errors and external disturbances are estimated together by using a nonlinear disturbance observer. The coupler design between the disturbance observer and RBFNN is analyzed in this paper. Command filters and auxiliary systems [35] are designed to avoid ''explosion of complexity'' in the backstepping control. The tracking errors of the control system can converge to a small neighborhood around zero in finite time, while the position error constraint can never be violated. The main contributions of this paper can be summarized as follows:

1) The position tracking error of the underactuated MSV can be strictly regulated to the prescribed constraint based on BLF control, which has practical significance for the safe navigation of MSVs.

2) Adaptive RBFNN is constructed to estimate the unknown hydrodynamic damping term of a vessel, and a nonlinear disturbance observer is designed to compensate for the compound disturbances in order to achieve a more accurate tracking performance.

3) In comparison with the controllers to achieve ultimately bounded stability in [10] and [17], the tracking errors of the vessel system in this paper can converge to a small neighborhood around the origin in finite-time.

The remainder of this paper is organized as follows. The preliminaries and problem formulation are introduced in Section 2. Section 3 is devoted to the finite-time trajectory tracking controllers design for a MSV. Numerical simulation results are given in Section 4. Section 5 concludes the paper.

II. PRELIMINARIES AND PROBLEM FORMULATION

A. PRELIMINARIES

Notation: Throughout this paper, $(\cdot)^T$ denotes the transpose of a matrix $(\cdot)$, $|\cdot|$ represents the absolute value of a scalar, $\|\cdot\|$ represents the Euclidean norm of a vector. For $a \in \mathbb{R}$, define $sig^{\gamma}(a) = |a|^{\gamma} \cdot sign(a)$.

Lemma 1 [22]: For any real numbers $\lambda_1 > 0, \lambda_2 > 0, 0 < l < 1$, an extended Lyapunov condition of finite-time stability can be given in the form $\dot{V}(x) + \lambda_1 V(x) + \lambda_2 V^l(x) \leq 0$, where the settling time can be estimated by

$$T_0 \leq \frac{1}{\lambda_1 (1-l)} \ln \frac{\lambda_1 V^{1-l}(x_0) + \lambda_2}{\lambda_2} \tag{1}$$

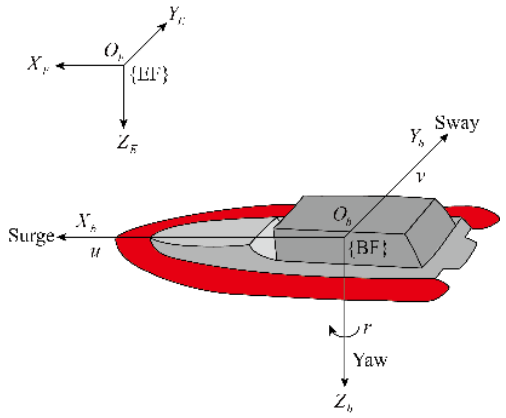

FIGURE 1. Coordinate frames of a MSV.

Lemma 2 [33]: If $0 < p < 1$, then the following inequality holds,

$$\sum_{i=1}^{n} |x_i|^{1+p} \geq \left(\sum_{i=1}^{n} |x_i|^2\right)^{(1+p)/2} \tag{2}$$

Lemma 3 [27]: Let m, n, and ι be positive real numbers, then for any real variables z and β, there exists

$$|z|^m|\beta|^n \leq \frac{m}{m+n}\iota|z|^{m+n} + \frac{n}{m+n}\iota^{-m/n}|\beta|^{m+n} \tag{3}$$

Lemma 4 [36]: For an unknown continuous nonlinear function $f(\boldsymbol{x}) : \mathbb{R}^m \to \mathbb{R}$, the radial basis function NN can be used to approximate it over a compact set $\Omega \subseteq \mathbb{R}^m$ as follows:

$$f(\boldsymbol{x}) = \boldsymbol{W}^{*T}\boldsymbol{H}(\boldsymbol{x}) + \varepsilon(\boldsymbol{x}) \tag{4}$$

where $x \in \mathbb{R}^m$ is the input vector of the NN, $\boldsymbol{W}^* = \left[w_1^*, \cdots, w_n^*\right]^T \in \mathbb{R}^n$ denotes the NN optimal weight vector. The hidden node number of the NN is n. $\varepsilon(\boldsymbol{x})$ is the optimal approximation error satisfying $|\varepsilon(\boldsymbol{x})| \leq \bar{\varepsilon}$, where $\bar{\varepsilon}$ is an unknown positive constant. The unknown optimal weight value $\boldsymbol{W}^*$ is calculated by

$$\boldsymbol{W}^* = \arg\min_{\hat{\boldsymbol{W}}} \left\{\sup_{\boldsymbol{x}\in\Omega} \left|f(\boldsymbol{x}) - \hat{\boldsymbol{W}}^T H(\boldsymbol{x})\right|\right\}$$

where $\hat{\boldsymbol{W}}$ represents the estimation of $\boldsymbol{W}^*$, which is usually obtained by an adaptive rule based on Lyapunov stability theorem. $\boldsymbol{H}(\boldsymbol{x}) = [h_1(\boldsymbol{x}), \cdots, h_n(\boldsymbol{x})]^T : \Omega \to \mathbb{R}^n$ is the radial basis function vector, and $h_i(\boldsymbol{x})$ are chosen as the Gaussian function in the following form:

$$h_i(\boldsymbol{x}) = \exp\left(-\frac{\|\boldsymbol{x} - \boldsymbol{\phi}_i\|^2}{\delta_i^2}\right), \quad (i = 1, 2, \cdots n)$$

where $\boldsymbol{\phi}_i \in \mathbb{R}^m$ and $\delta_i \in \mathbb{R}$ are the center and width of the radial basis function, respectively. According to its definition, we know that there exists a positive constant such that $\|\boldsymbol{H}(\boldsymbol{x})\| \leq \mu$ with $\mu > 0$.

B. DYNAMIC MODEL OF AN UNDERACTUATED MSV

For motion control of a 3-DOF underactuated MSV, two reference frames, the earth-fixed frame (EF) $O_EX_EY_EZ_E$ and the body-fixed frame (BF) $O_bX_bY_bZ_b$, are defined in Fig. 1. The origin O_E of EF is fixed to the earth. O_EX_E-axis is directed to north, O_EY_E-axis is directed to east. The origin O_b of the BF is assumed to locate in the vessel center of mass (CG). The body axes O_bX_b is directed from aft to fore, O_bY_b is directed to right starboard. Neglecting the heave, roll and pitch motion, the dynamic mode of an underactuated vessel subject to external ocean disturbances can be described as follows:

$$\begin{cases} \dot{x} = u\cos(\psi) - v\sin(\psi) \\ \dot{y} = u\sin(\psi) + v\cos(\psi) \\ \dot{\psi} = r \end{cases} \tag{5}$$

where $\boldsymbol{\eta} = [x, y, \psi]^T$ denotes the MSV position and heading angle with respect to EF. $\boldsymbol{\nu} = [u, v, r]^T$ denotes the linear velocities and angular rate in BF, respectively.

The dynamics model of the vessel is described by [4]:

$$\begin{cases} \dot{u} = \dfrac{m_{22}}{m_{11}}vr - f_u(u) + \dfrac{1}{m_{11}}\tau_u + \dfrac{1}{m_{11}}\tau_{wu} \\ \dot{v} = -\dfrac{m_{11}}{m_{22}}ur - f_v(v) + \dfrac{1}{m_{22}}\tau_{wv} \\ \dot{r} = \dfrac{m_{11} - m_{22}}{m_{33}}uv - f_r(r) + \dfrac{1}{m_{33}}\tau_r + \dfrac{1}{m_{33}}\tau_{wr} \end{cases} \tag{6}$$

with

$$\begin{aligned} f_u(u) &= \frac{d_u}{m_{11}}u + \sum_{i=2}^{3}\frac{d_{ui}}{m_{11}}|u|^{i-1}u \\ f_v(v) &= \frac{d_v}{m_{22}}v + \sum_{i=2}^{3}\frac{d_{vi}}{m_{22}}|v|^{i-1}v \\ f_r(r) &= \frac{d_r}{m_{33}}r + \sum_{i=2}^{3}\frac{d_{ri}}{m_{33}}|r|^{i-1}r \end{aligned} \tag{7}$$

where m_{ii}, $i = 1, 2, 3$ denote the combined inertia and added mass of a vessel. Parameters d_u, d_v, d_r, d_{ui}, d_{vi} and d_{ri} denote the hydrodynamic damping coefficients, which can be obtained by using system identification based on the experimental data. Here, we assume that the hydrodynamic damping term $f_u(u), f_v(v)$ and $f_r(r)$ are completely unknown. The control inputs are the surge force τ_u and yaw moment τ_r. In addition, τ_{wu}, τ_{wv} and τ_{wr} represent the bounded time-varying ocean disturbances induced by winds, waves and ocean currents, respectively.

C. CONTROL OBJECTIVE

The desired trajectory to be tracked is generated by a virtual vessel as follows

$$\begin{cases} \dot{x}_d = u_d\cos(\psi_d) - v_d\sin(\psi_d) \\ \dot{y}_d = u_d\sin(\psi_d) + v_d\cos(\psi_d) \\ \dot{\psi}_d = r_d \end{cases} \tag{8}$$

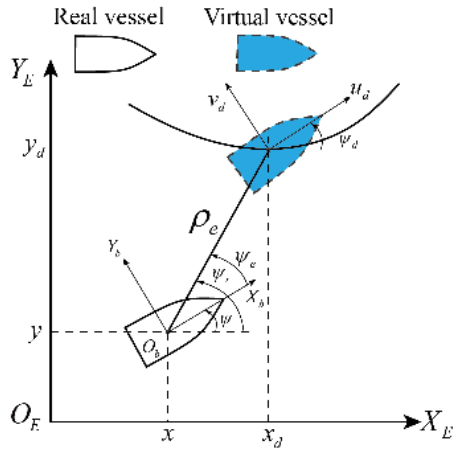

FIGURE 2. Definition of tracking errors.

where $\boldsymbol{\eta}_d = [x_d, y_d, \psi_d]^T$ are the desired position and heading angle. (u_d, v_d, r_d) are the desired velocities of the virtual vessel with respect to BF, and the tracking errors are illustrated in Fig. 2.

Assumption 1: The reference trajectories generated by (8) should be smooth enough, such that $x_d, \dot{x}_d, \ddot{x}_d, y_d, \dot{y}_d, \ddot{y}_d, \psi_d, \dot{\psi}_d, \ddot{\psi}_d$ are all bounded.

According to Fig. 2, we define the tracking errors as follows

$$\begin{aligned} x_e &= x_d - x, \quad y_e = y_d - y \\ \psi_e &= \psi_r - \psi, \quad \rho_e = \sqrt{x_e^2 + y_e^2} \end{aligned} \tag{9}$$

where ρ_e denotes the distance between the CG of the real vessel and virtual vessel. ψ_r is the azimuth angle of the vessel, which is related to the position of the virtual vessel and defined as follows [37]:

$$\psi_r = \frac{1}{2}\pi \left[1 - sgn\left(x_e\right)\right] sgn\left(y_e\right) + \arctan\left(\frac{y_e}{x_e}\right) \tag{10}$$

Remark 1: It can be seen from (10) that $\psi_r \in (-\pi, \pi]$. Moreover, we have $\arctan(y_e/x_e) \to \pm\frac{\pi}{2}$ if $y_e \neq 0$ and $x_e = 0$. However, $\arctan\left(y_e/x_e\right)$ is not defined when the position error $\rho_e = 0$. Therefore, we set $\psi_r = \psi_d$ when $\rho_e = 0$.

The control objective in this study is to design an adaptive neural-based tracking controller for an underactuated vessel subject to model uncertainties and external disturbances such that:

(i) The reference trajectory (x_d, y_d, ψ_r) can be tracked as closely as possible, while the constraint on the position tracking error ρ_e can be strictly guaranteed, i.e., $|\rho_e| < k_e$ holds for all $t \geq 0$, where k_e is the predefined constraint.

(ii) The tracking errors of the vessel control system can converge to arbitrarily small ranges around zero within finite time, and all closed-loop signals are bounded.

To facilitate the trajectory tracking control design, the following assumptions are necessary:

Assumption 2: The external disturbances τ_{wu}, τ_{wv} and τ_{wr} are unknown but bounded, and their first derivatives are also bounded.

Assumption 3 [37]: The sway velocity v of an underactuated vessel is passive-bounded $\forall t \geq 0$ in the sense that $\sup_{t\geq 0} |v(t)| \leq \lambda_v$, where λ_v is an unknown positive constant.

III. CONTROL SYSTEM DESIGN

In this section, a constrained finite-time trajectory tracking controller will be designed for an underactuated vessel based on barrier Lyapunov function, adaptive NN control and finite-time theory. The control scheme consists of two subsystems: surge motion control and yaw motion control. Finally, the Lyapunov stability analysis is carried out for the proposed controller.

A. POSITION CONTROL

According to (9) and Fig. 2, one can obtain

$$\begin{cases} x_e = \rho_e \cos\left(\psi_r\right), \quad y_e = \rho_e \sin\left(\psi_r\right) \end{cases} \tag{11}$$

Taking the time derivative of ρ_e along (5), (9) and (11) yields

$$\begin{aligned} \dot{\rho}_e &= \left(x_e \dot{x}_e + y_e \dot{y}_e\right) / \rho_e \\ &= \dot{x}_e \cos\left(\psi_r\right) + \dot{y}_e \sin\left(\psi_r\right) \\ &= \left(\dot{x}_d - u\cos\left(\psi\right) + v\sin\left(\psi\right)\right)\cos\left(\psi_r\right) + \left(\dot{y}_d \right. \\ &\quad \left. - u\sin\left(\psi\right) - v\cos\left(\psi\right)\right)\sin\left(\psi_r\right) \\ &= \dot{x}_d \cos\left(\psi_r\right) + \dot{y}_d \sin\left(\psi_r\right) - u\cos\left(\psi_e\right) \\ &\quad - v\sin\left(\psi_e\right) \end{aligned} \tag{12}$$

Step 1: To guarantee the position error constraint on ρ_e, we choose a logarithmic barrier Lyapunov function as follows:

$$V_\rho = \frac{1}{2}\log\frac{k_e^2}{k_e^2 - \rho_e^2} \tag{13}$$

which satisfies that V_ρ is positive definite and continuous, and $V_\rho = 0$ if and only if $\rho_e = 0$ in the set $|\rho_e| < k_e$. The time derivative of V_ρ can be calculated as

$$\dot{V}_\rho = \xi_\rho \dot{\rho}_e \tag{14}$$

with $\xi_\rho = \frac{\rho_e}{k_e^2 - \rho_e^2}$.

Defining the error variable $u_e = \alpha_u - u$ and $\Delta\alpha_u = \alpha_u - \alpha_{u,c}$, where $\Delta\alpha_u$ is the filter error of the command filter. Substituting (12) into (14) yields

$$\begin{aligned} \dot{V}_\rho = \xi_\rho &\left(\dot{x}_d \cos\left(\psi_r\right) + \dot{y}_d \sin\left(\psi_r\right) - \alpha_{u,c}\cos\left(\psi_e\right)\right. \\ &\left. - \Delta\alpha_u \cos\left(\psi_e\right) + u_e \cos\left(\psi_e\right) - v\sin\left(\psi_e\right)\right) \end{aligned} \tag{15}$$

The nominal virtual control law is designed as

$$\begin{aligned} \alpha_{u,c} = &\left(\dot{x}_d \cos\left(\psi_r\right) + \dot{y}_d \sin\left(\psi_r\right) - v\sin\left(\psi_e\right) + k_1\rho_e \right. \\ &\left. + k_2 \frac{\rho_e^{2l-1}}{\left(k_e^2 - \rho_e^2\right)^{l-1}} - k_m e_1 + \frac{k_m^2}{2}\xi_\rho\right) / \cos\left(\psi_e\right) \end{aligned} \tag{16}$$

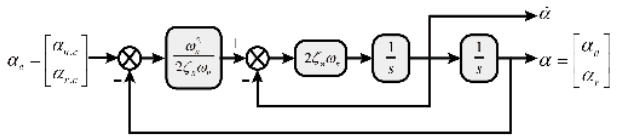

FIGURE 3. Configuration of the command filter.

where k_1, k_2 and k_m are positive design parameters. $0 < l < 1$. e_1 is the state of the auxiliary system to compensate for the error $\Delta\alpha_u$, and the auxiliary system will be designed later.

Remark 2: Note that the virtual control law $\alpha_{u,c}$ is not well defined when $\psi_e = \pm\frac{\pi}{2}$. To avoid singularity occurs in (16), we can use $sgn(\cos(\psi_e))\kappa$ to replace the denominator of $\alpha_{u,c}$ when $|\cos(\psi_e)| < \kappa$, where κ is a small positive constant. ψ_e is transformed to locate in the domain $\left[-\frac{\pi}{2}, \frac{\pi}{2}\right]$ by the following rules [17]:

$$\psi_e = \begin{cases} \psi_e - \pi, & \psi_e \geq \pi/2 \\ \psi_e, & -\pi/2 < \psi_e < \pi/2 \\ \psi_e + \pi, & \psi_e \leq -\pi/2 \end{cases} \tag{17}$$

To generate the virtual control law α_u and its time derivative $\dot{\alpha}_u$, we let the nominal virtual control law $\alpha_{u,c}$ pass through a second-order command filter as depicted in Fig. 3. Based on Fig. 3, let $\boldsymbol{x}_1 = \boldsymbol{\alpha}$ and $\boldsymbol{x}_2 = \dot{\boldsymbol{\alpha}}$, the command filter can be expressed as

$$\begin{cases} \dot{\boldsymbol{x}}_1 = \boldsymbol{x}_2 \\ \dot{\boldsymbol{x}}_2 = -2\zeta_n\omega_n\left(\boldsymbol{x}_2 + \dfrac{\omega_n^2}{2\zeta_n\omega_n}(\boldsymbol{x}_1 - \boldsymbol{\alpha}_c)\right) \end{cases} \tag{18}$$

where ζ_n and ω_n are the filter parameters.

Next, the auxiliary system will be designed to compensate for the estimation error $\Delta\alpha_u$. Denote that

$$f_1 = \frac{\left|\xi_\rho \Delta\alpha_u \cos\psi_e\right| + 0.5\gamma_1^2\Delta\alpha_u^2}{|e_1|^2}$$

for $|e_1| \neq 0$, $\gamma_1 > 0$. The auxiliary system is designed as

$$\dot{e}_1 = \begin{cases} -k_{c1}e_1 - k_{c2}sig^{2l-1}(e_1) \\ \quad -f_1e_1 + \gamma_1\Delta\alpha_u, & |e_1| > \kappa_1 \\ 0, & |e_1| \leq \kappa_1 \end{cases} \tag{19}$$

where e_1 is the state of the auxiliary system (19). $k_{c1} > 1$, k_{c2} is a positive design constant. κ_1 is a sufficiently small constant, which can be adjusted to satisfy the required control performance.

Define the Lyapunov function as follows:

$$V_1 = V_\rho + \frac{1}{2}e_1^2 \tag{20}$$

Substituting (16) into (15) and using (19), the time derivative of (20) is calculated as

$$\begin{aligned} \dot{V}_1 = \xi_\rho\Bigg(& -k_1\rho_e - k_2\frac{\rho_e^{2l-1}}{\left(k_e^2 - \rho_e^2\right)^{l-1}} + k_me_1 - \frac{k_m^2}{2}\xi_\rho^2 \\ & - \Delta\alpha_u\cos(\psi_e) + u_e\cos(\psi_e)\Bigg) + e_1\Big(- k_{c1}e_1 \\ & - k_{c2}sig^{2l-1}(e_1) - f_1e_1 + \gamma_1\Delta\alpha_u\Big) \\ \leq & -k_1\frac{\rho_e^2}{k_e^2 - \rho_e^2} - k_2\frac{\rho_e^{2l}}{\left(k_e^2 - \rho_e^2\right)^l} - (k_{c1} - 1)e_1^2 \\ & - k_{c2}|e_1|^{2l} + \xi_\rho u_e\cos(\psi_e) \end{aligned} \tag{21}$$

Step 2: In this step, the control objective is to design the surge control force τ_u so that to stabilize u_e. The time derivative of u_e is calculated as

$$\dot{u}_e = \dot{\alpha}_u - \frac{m_{22}}{m_{11}}vr + f_u(u) - \frac{1}{m_{11}}\tau_u - \frac{1}{m_{11}}\tau_{wu} \tag{22}$$

Since $f_u(u)$ is an unknown continuous function, RBFNN is adopted to approximate this term. According to Lemma 4, we have

$$f_u(u) = p_1^{-1}\boldsymbol{W}_1^{*T}\boldsymbol{H}_1(\boldsymbol{v}) + p_1^{-1}\varepsilon_1(\boldsymbol{v}) \tag{23}$$

where p_1 is the design parameter. $|\varepsilon_1(\boldsymbol{v})| \leq \bar{\varepsilon}_1$, $\bar{\varepsilon}_1$ is a positive constant.

Invoking (23) into (22), we obtain

$$\begin{aligned} \dot{u}_e = \dot{\alpha}_u - \frac{m_{22}}{m_{11}}vr + p_1^{-1}\boldsymbol{W}_1^{*T}\boldsymbol{H}_1(\boldsymbol{v}) + p_1^{-1}\varepsilon_1 \\ - \frac{1}{m_{11}}\tau_u - \frac{1}{m_{11}}\tau_{wu} \end{aligned} \tag{24}$$

In (24), we define the compound disturbance as $D_u = p_1^{-1}\varepsilon_1(\boldsymbol{v}) - \frac{1}{m_{11}}\tau_{wu}$. According to Assumption 2, we know that the lumped time-varying disturbance $D_u(t)$ is unknown but bounded. In addition, in light of the approximation theory of NN [38], we have $\dot{\varepsilon}_1$ is bounded. Thus, the time derivative of $D_u(t)$ satisfies

$$\left|\dot{D}_u(t)\right| \leq \bar{D}_u \tag{25}$$

where $\bar{D}_u$ is an unknown positive constant.

Consider the Lyapunov function as follows

$$V_2 = \frac{1}{2}u_e^2 + \frac{1}{2}\tilde{\boldsymbol{W}}_1^T\boldsymbol{\Gamma}_1^{-1}\tilde{\boldsymbol{W}}_1 + \frac{1}{2}\tilde{D}_u^2 \tag{26}$$

where $\tilde{\boldsymbol{W}}_1$ and $\tilde{D}_u$ represent the neural approximation error and the disturbance estimation error, respectively, which are defined as $\tilde{\boldsymbol{W}}_1 = \boldsymbol{W}_1^* - \hat{\boldsymbol{W}}_1$ and $\tilde{D}_u = D_u - \hat{D}_u$. $\hat{\boldsymbol{W}}_1$ and $\hat{D}_u$ denote the estimate values of $\boldsymbol{W}_1^*$ and D_u, respectively. $\boldsymbol{\Gamma}_1 = \boldsymbol{\Gamma}_1^T > 0$ is a positive definite matrix.

Differentiating (26) with respect to time and invoking (24) yields

$$\begin{aligned} \dot{V}_2 = u_e\left(\dot{\alpha}_u - \frac{m_{22}}{m_{11}}vr + p_1^{-1}\boldsymbol{W}_1^{*T}\boldsymbol{H}_1(\boldsymbol{v}) - \frac{1}{m_{11}}\tau_u + D_u\right) \\ - \tilde{\boldsymbol{W}}_1^T\boldsymbol{\Gamma}_1^{-1}\dot{\hat{\boldsymbol{W}}}_1 + \tilde{D}_u\dot{D}_u - \tilde{D}_u\dot{\hat{D}}_u \end{aligned} \tag{27}$$

Now, we design the surge tracking controller as follows:

$$\begin{aligned} \tau_u = m_{11}\Big(k_3u_e + k_4sig^{2l-1}(u_e) + \hat{D}_u + \dot{\alpha}_u \\ + \xi_\rho\cos(\psi_e) + p_1^{-1}\hat{\boldsymbol{W}}_1^T\boldsymbol{H}_1(\boldsymbol{v})\Big) - m_{22}vr \end{aligned} \tag{28}$$

where k_3 and k_4 are positive design constants. $\dot{\alpha}_u$ is directly obtained from the command filter (18).

The adaptive law of the RBFNN weight vector $\hat{\boldsymbol{W}}_1$ is designed as

$$\dot{\hat{\boldsymbol{W}}}_1 = \boldsymbol{\Gamma}_1 \left(p_1^{-1} \boldsymbol{H}_1 (\boldsymbol{v})\, u_e - \sigma_1 \hat{\boldsymbol{W}}_1 \right) \tag{29}$$

where $\sigma_1 > 2$ is a positive design parameter.

To compensate for the compound disturbance $D_u(t)$, a nonlinear disturbance observer is designed as follows:

$$\begin{cases} \hat{D}_u = \vartheta_1 - p_1 u \\ \dot{\vartheta}_1 = -p_1 \vartheta_1 + p_1 \left(\dfrac{m_{22}}{m_{11}} vr - p_1^{-1} \hat{\boldsymbol{W}}_1^T \boldsymbol{H}_1 (\boldsymbol{v}) \right. \\ \left. + \dfrac{1}{m_{11}} \tau_u + p_1 u \right) + u_e \end{cases} \tag{30}$$

where ϑ_1 is the state of the disturbance observer. The disturbance observer (30) is a dynamical system. The derivative of ϑ_1 is obtained based on a proper design of the control input τ_u, the available vessel states $\boldsymbol{v}$ and the estimation value of RBFNN. Given a certain initial value $\vartheta_1(0)$, the variable ϑ_1 can be generated by the constructed ordinary differential equation in (30).

Based on (6) and (30), we have

$$\begin{aligned} -\tilde{D}_u \dot{\hat{D}}_u &= -\tilde{D}_u \left(\dot{\vartheta}_1 - p_1 \dot{u} \right) \\ &= -\tilde{D}_u \left(-p_1 \vartheta_1 + p_1 \left(\frac{m_{22}}{m_{11}} vr - p_1^{-1} \hat{\boldsymbol{W}}_1^T \boldsymbol{H}_1 (\boldsymbol{v}) \right. \right. \\ &\quad \left. \left. + \frac{1}{m_{11}} \tau_u + p_1 u \right) + u_e - p_1 \dot{u} \right) \\ &= -\tilde{D}_u \left(p_1 \tilde{D}_u + u_e + \tilde{\boldsymbol{W}}_1^T \boldsymbol{H}_1 (\boldsymbol{v}) \right) \\ &= -p_1 \tilde{D}_u^2 - \tilde{D}_u u_e - \tilde{D}_u \tilde{\boldsymbol{W}}_1^T \boldsymbol{H}_1 (\boldsymbol{v}) \end{aligned} \tag{31}$$

Substituting (28), (29) and (31) into (27) results in

$$\begin{aligned} \dot{V}_2 &= u_e \Big(-k_3 u_e - k_4 sig^{2l-1}(u_e) - \xi_\rho \cos(\psi_e) \\ &\quad + p_1^{-1} \tilde{\boldsymbol{W}}_1^T \boldsymbol{H}_1 (\boldsymbol{v}) + \tilde{D}_u \Big) - p_1^{-1} \tilde{\boldsymbol{W}}_1^T \boldsymbol{H}_1 (\boldsymbol{v})\, u_e \\ &\quad + \sigma_1 \tilde{\boldsymbol{W}}_1^T \hat{\boldsymbol{W}} + \tilde{D}_u \dot{D}_u - p_1 \tilde{D}_u^2 - \tilde{D}_u u_e \\ &\quad - \tilde{D}_u \tilde{\boldsymbol{W}}_1^T \boldsymbol{H}_1 (\boldsymbol{v}) \\ &\le -k_3 u_e^2 - k_4 |u_e|^{2l} - u_e \xi_\rho \cos(\psi_e) + \sigma_1 \tilde{\boldsymbol{W}}_1^T \hat{\boldsymbol{W}} \\ &\quad + \tilde{D}_u \dot{D}_u - p_1 \tilde{D}_u^2 - \tilde{D}_u \tilde{\boldsymbol{W}}_1^T \boldsymbol{H}_1 (\boldsymbol{v}) \end{aligned} \tag{32}$$

Noting $\|\boldsymbol{H}_1(\boldsymbol{v})\| \le \mu_1$ with $\mu_1 > 0$, the following inequality holds:

$$\begin{aligned} -\tilde{D}_u \tilde{\boldsymbol{W}}_1^T \boldsymbol{H}_1 (\boldsymbol{v}) &\le \mu_1 \left| \tilde{D}_u \right| \left\| \tilde{\boldsymbol{W}}_1 \right\| \\ &\le \frac{\mu_1^2}{2} \tilde{D}_u^2 + \frac{1}{2} \tilde{\boldsymbol{W}}_1^T \tilde{\boldsymbol{W}}_1 \end{aligned} \tag{33}$$

By using Young's inequality, we obtain

$$\begin{aligned} \sigma_1 \tilde{\boldsymbol{W}}_1^T \hat{\boldsymbol{W}}_1 &= \sigma_1 \tilde{\boldsymbol{W}}_1^T \left(\boldsymbol{W}_1^* - \tilde{\boldsymbol{W}}_1 \right) \\ &\le -\frac{\sigma_1 \tilde{\boldsymbol{W}}_1^T \tilde{\boldsymbol{W}}_1}{2} + \frac{\sigma_1 \boldsymbol{W}_1^{*T} \boldsymbol{W}_1^*}{2} \\ &= -\frac{\sigma_1 \tilde{\boldsymbol{W}}_1^T \tilde{\boldsymbol{W}}_1}{4} - \frac{\sigma_1}{4} \left(\tilde{\boldsymbol{W}}_1^T \tilde{\boldsymbol{W}}_1 \right)^l - \frac{\sigma_1 \tilde{\boldsymbol{W}}_1^T \tilde{\boldsymbol{W}}_1}{4} \\ &\quad + \frac{\sigma_1}{4} \left(\tilde{\boldsymbol{W}}_1^T \tilde{\boldsymbol{W}}_1 \right)^l + \frac{\sigma_1 \boldsymbol{W}_1^{*T} \boldsymbol{W}_1^*}{2} \end{aligned} \tag{34}$$

Note that if $\tilde{\boldsymbol{W}}_1^T \tilde{\boldsymbol{W}}_1 \ge 1$, we have $-\tilde{\boldsymbol{W}}_1^T \tilde{\boldsymbol{W}}_1 + \left(\tilde{\boldsymbol{W}}_1^T \tilde{\boldsymbol{W}}_1 \right)^l \le 0$. Otherwise, if $\tilde{\boldsymbol{W}}_1^T \tilde{\boldsymbol{W}}_1 < 1$, we have $-\tilde{\boldsymbol{W}}_1^T \tilde{\boldsymbol{W}}_1 + \left(\tilde{\boldsymbol{W}}_1^T \tilde{\boldsymbol{W}}_1 \right)^l < \Phi_1$, where $\Phi_1 = l^{\frac{l}{1-l}} - l^{\frac{1}{1-l}} > 0$. Therefore, for arbitrary $\tilde{\boldsymbol{W}}_1^T \tilde{\boldsymbol{W}}_1$, we can always obtain

$$\sup_{t \ge 0} \left\{ -\frac{\sigma_1 \tilde{\boldsymbol{W}}_1^T \tilde{\boldsymbol{W}}_1}{4} + \frac{\sigma_1}{4} \left(\tilde{\boldsymbol{W}}_1^T \tilde{\boldsymbol{W}}_1 \right)^l \right\} < \frac{\sigma_1}{4} \Phi_1 \tag{35}$$

Moreover, let $z = 1$, $\beta = \tilde{D}_u^2$, $m = 1 - l$, $n = l$, $\iota = l^{\frac{l}{1-l}}$. In light of Lemma 3, we have

$$\tilde{D}_u^{2l} \le (1 - l)\, \iota + \tilde{D}_u^2 \tag{36}$$

Furthermore, we can obtain

$$-\tilde{D}_u^2 \le -\frac{\tilde{D}_u^2}{2} - \frac{\tilde{D}_u^{2l}}{2} + \frac{(1 - l)\, \iota}{2} \tag{37}$$

Based on the inequalities (33), (34), (35) and (37), we can derive that (32) satisfies

$$\begin{aligned} \dot{V}_2 &\le -k_3 u_e^2 - k_4 |u_e|^{2l} - \left(\frac{\sigma_1}{4} - \frac{1}{2} \right) \tilde{\boldsymbol{W}}_1^T \tilde{\boldsymbol{W}}_1 \\ &\quad - \frac{\sigma_1}{4} \left(\tilde{\boldsymbol{W}}_1^T \tilde{\boldsymbol{W}}_1 \right)^l - \left(\frac{p_1}{2} - \frac{\mu_1^2}{4} - \frac{1}{4} \right) \tilde{D}_u^2 \\ &\quad - \left(\frac{p_1}{2} - \frac{\mu_1^2}{4} - \frac{1}{4} \right) \tilde{D}_u^{2l} - u_e \xi_\rho \cos(\psi_e) \\ &\quad + \frac{\sigma_1 \boldsymbol{W}_1^{*T} \boldsymbol{W}_1^*}{2} + \frac{\sigma_1}{4} \Phi_1 + \frac{\tilde{D}_u^2}{2} \\ &\quad + (1 - l) \left(\frac{p_1}{2} - \frac{\mu_1^2}{4} - \frac{1}{4} \right) \iota \end{aligned} \tag{38}$$

B. ATTITUDE CONTROL

Step 1: In this step, we will firstly design the virtual control law α_r to stabilize the tracking error ψ_e. Consider the following Lyapunov function

$$V_\psi = \frac{1}{2} \psi_e^2 \tag{39}$$

Taking the time derivative of (39) along (5) and (10) yields

$$\dot{V}_\psi = \psi_e \left(\dot{\psi}_r - r \right) \tag{40}$$

Define the error variables $r_e = \alpha_r - r$ and $\Delta\alpha_r = \alpha_r - \alpha_{r,c}$, where $\Delta\alpha_r$ is the filter error. Thus, we have

$$\dot{V}_\psi = \psi_e \left(\dot{\psi}_r - \Delta\alpha_r - \alpha_{r,c} + r_e \right) \tag{41}$$

The nominal virtual control law for ψ_e is designed as

$$\alpha_{r,c} = \dot{\psi}_r + k_5 \psi_e + k_6 sig^{2l-1}(\psi_e) - k_n e_2 + \frac{k_n^2}{2} \psi_e \tag{42}$$

where k_5, k_6 and k_n are positive design constants. e_2 is the state of the auxiliary system. In order to avoid the tedious derivative computation of the virtual control law α_r, we let $\alpha_{r,c}$ pass through the command filter as shown in Fig. 3 to generate α_r and its time derivative. The auxiliary system is designed as

$$\dot{e}_2 = \begin{cases} -k_{c3}e_2 - k_{c4}sig^{2l-1}(e_2) \\ \quad -f_2 e_2 + \gamma_2 \Delta\alpha_r, & |e_2| > \kappa_2 \\ 0, & |e_2| \le \kappa_2 \end{cases} \tag{43}$$

with

$$f_2 = \frac{|\psi_e \Delta\alpha_r| + 0.5\gamma_2^2 \Delta\alpha_r^2}{|e_2|^2}$$

where $k_{c3} > 1$ and k_{c4} is a positive design parameter. $\gamma_2 > 0$. κ_2 is a small region that can be adjusted to satisfy the required control performance.

Constructing the Lyapunov function as follows

$$V_3 = V_\psi + \frac{1}{2}e_2^2 \tag{44}$$

Using (41), (42) and (43), the time derivative of (44) is calculated as

$$\begin{aligned} \dot{V}_3 &= \dot{V}_\psi + e_2\dot{e}_2 \\ &= \psi_e\Big(- k_5\psi_e - k_6 sig^{2l-1}(\psi_e) + r_e - \Delta\alpha_r + k_n e_2 \\ &\quad - \frac{k_n^2}{2}\psi_e\Big) + e_2\big(- k_{c3}e_2 - k_{c4}sig^{2l-1}(e_2) - f_2 e_2 \\ &\quad + \gamma_2\Delta\alpha_r\big) \\ &\le -k_5\psi_e^2 - k_6|\psi_e|^{2l} - k_{c3}e_2^2 - k_{c4}|e_2|^{2l} + \psi_e r_e \\ &\quad + k_n\psi_e e_2 - \frac{k_n^2}{2}\psi_e^2 - \frac{1}{2}\gamma_2^2\Delta\alpha_r^2 + \gamma_2\Delta\alpha_r e_2 \\ &\le -k_5\psi_e^2 - k_6|\psi_e|^{2l} - (k_{c3}-1)e_2^2 - k_{c4}|e_2|^{2l} + \psi_e r_e \end{aligned} \tag{45}$$

Step 2: The time derivative of r_e along (6) and (42) is calculated as

$$\dot{r}_e = \dot{\alpha}_r - \frac{m_{11}-m_{22}}{m_{33}}uv + f_r(r) - \frac{1}{m_{33}}\tau_r - \frac{1}{m_{33}}\tau_{wr} \tag{46}$$

In (46), $f_r(r)$ is the unknown hydrodynamic damping term, which is unavailable for the control design. RBFNN is adopted to estimate $f_r(r)$, based on (4), the estimate output is given as

$$f_r(r) = p_2^{-1}\boldsymbol{W}_2^{*T}\boldsymbol{H}_2(\boldsymbol{v}) + p_2^{-1}\varepsilon_2(\boldsymbol{v}) \tag{47}$$

where p_2 is a positive constant.

Substituting (47) into (46) yields

$$\dot{r}_e = \dot{\alpha}_r - \frac{m_{11}-m_{22}}{m_{33}}uv + p_2^{-1}\boldsymbol{W}_2^{*T}\boldsymbol{H}_2(\boldsymbol{v}) - \frac{1}{m_{33}}\tau_r + D_r(t) \tag{48}$$

where $D_r(t) = p_2^{-1}\varepsilon_2(\boldsymbol{v}) - \frac{1}{m_{33}}\tau_{wr}$. Since $|\varepsilon_2(\boldsymbol{v})| \le \bar{\varepsilon}_2$ and τ_{wr} is bounded, it can be obtained that $D_r(t)$ is bounded. Based on the approximation theory of NN, we know $\dot{\varepsilon}_2$ is bounded. Thus, we assume

$$\left|\dot{D}_r(t)\right| \le \bar{D}_r \tag{49}$$

where $\bar{D}_r$ is an unknown positive constant.

Construct the following Lyapunov function:

$$V_4 = \frac{1}{2}r_e^2 + \frac{1}{2}\tilde{\boldsymbol{W}}_2^T\boldsymbol{\Gamma}_2^{-1}\tilde{\boldsymbol{W}}_2 + \frac{1}{2}\tilde{D}_r^2 \tag{50}$$

where $\tilde{\boldsymbol{W}}_2$ and $\tilde{D}_r$ denote the estimation errors, which are defined as $\tilde{\boldsymbol{W}}_2 = \boldsymbol{W}_2^* - \hat{\boldsymbol{W}}_2$, $\tilde{D}_r = D_r - \hat{D}_r$. $\hat{\boldsymbol{W}}_2$ and $\hat{D}_r$ are the estimation values of $\boldsymbol{W}_2^*$ and D_r, respectively. Taking the time derivative of (50), one can obtain

$$\begin{aligned} \dot{V}_4 = r_e\Big(\dot{\alpha}_r - \frac{m_{11}-m_{22}}{m_{33}}uv + p_2^{-1}\boldsymbol{W}_2^{*T}\boldsymbol{H}_2(\boldsymbol{v}) \\ - \frac{1}{m_{33}}\tau_r + D_r(t)\Big) - \tilde{\boldsymbol{W}}_2^T\boldsymbol{\Gamma}_2^{-1}\dot{\hat{\boldsymbol{W}}}_2 + \tilde{D}_r\dot{D}_r - \tilde{D}_r\dot{\hat{D}}_r \end{aligned} \tag{51}$$

Then, the yaw control law is designed as follows:

$$\begin{aligned} \tau_r = m_{33}\Big(k_7 r_e + k_8 sig^{2l-1}(r_e) + \dot{\alpha}_r + p_2^{-1}\hat{\boldsymbol{W}}_2^T\boldsymbol{H}_2(\boldsymbol{v}) \\ + \hat{D}_r + \psi_e\Big) - (m_{11}-m_{22})uv \end{aligned} \tag{52}$$

where k_7 and k_8 are positive design constants. $\dot{\alpha}_r$ is directly obtained from (18) according to the stabilizing function $\alpha_{r,c}$.

The adaptive law for $\hat{\boldsymbol{W}}_2$ is chosen as

$$\dot{\hat{\boldsymbol{W}}}_2 = \boldsymbol{\Gamma}_2\left(p_2^{-1}\boldsymbol{H}_2(\boldsymbol{v})r_e - \sigma_2\hat{\boldsymbol{W}}_2\right) \tag{53}$$

where $\sigma_2 > 2$ is a designed parameter.

To estimate and compensate for the lumped disturbance D_r, the disturbance observer is designed as follows:

$$\begin{cases} \hat{D}_r = \vartheta_2 - p_2 r \\ \dot{\vartheta}_2 = -p_2\vartheta_2 + p_2\left(\frac{m_{11}-m_{22}}{m_{33}}uv - p_2^{-1}\hat{\boldsymbol{W}}_2^T\boldsymbol{H}_2(\boldsymbol{v})\right. \\ \left. + \frac{1}{m_{33}}\tau_r + p_2 r\right) + r_e \end{cases} \tag{54}$$

where ϑ_2 is the state of the disturbance observer. According to (6) and (54), we can obtain

$$\begin{aligned} -\tilde{D}_r\dot{\hat{D}}_r &= -\tilde{D}_r\left(\dot{\vartheta}_2 - p_2\dot{r}\right) \\ &= -\tilde{D}_r\Big(p_2\Big(\frac{m_{11}-m_{22}}{m_{33}}uv - p_2^{-1}\hat{\boldsymbol{W}}_2^T\boldsymbol{H}_2(\boldsymbol{v}) \\ &\quad + \frac{1}{m_{33}}\tau_r + p_2 r\Big) - p_2\vartheta_2 + r_e - p_2\dot{r}\Big) \\ &= -\tilde{D}_r\left(p_2\tilde{D}_r + r_e + \tilde{\boldsymbol{W}}_2^T\boldsymbol{H}_2(\boldsymbol{v})\right) \\ &= -p_2\tilde{D}_r^2 - \tilde{D}_r r_e - \tilde{D}_r\tilde{\boldsymbol{W}}_2^T\boldsymbol{H}_2(\boldsymbol{v}) \end{aligned} \tag{55}$$

Substituting (52), (53) and (55) into (51), the time derivative of V_4 satisfies

$$V_4 = \frac{1}{2}r_e^2 + \frac{1}{2}\tilde{\boldsymbol{W}}_2^T\boldsymbol{\Gamma}_2^{-1}\tilde{\boldsymbol{W}}_2 + \frac{1}{2}\tilde{D}_r^2$$

$$
\begin{aligned}
&= r_e\left(-k_7 r_e - k_8 sig^{2l-1}(r_e) - \psi_e + p_2^{-1}\tilde{\boldsymbol{W}}_2^T\boldsymbol{H}_2(\boldsymbol{v})\right.\\
&\quad\left.+\tilde{D}_r\right) - p_2^{-1}\tilde{\boldsymbol{W}}_2^T\boldsymbol{H}_2(\boldsymbol{v})\, r_e + \sigma_2\tilde{\boldsymbol{W}}_2^T\hat{\boldsymbol{W}}_2 + \tilde{D}_r\dot{D}_r\\
&\quad - p_2\tilde{D}_r^2 - \tilde{D}_r r_e - \tilde{D}_r\tilde{\boldsymbol{W}}_2^T\boldsymbol{H}_2(\boldsymbol{v})\\
&\le -k_7 r_e^2 - k_8|r_e|^{2l} - r_e\psi_e + \sigma_2\tilde{\boldsymbol{W}}_2^T\hat{\boldsymbol{W}}_2\\
&\quad + \tilde{D}_r\dot{D}_r - p_2\tilde{D}_r^2 - \tilde{D}_r\tilde{\boldsymbol{W}}_2^T\boldsymbol{H}_2(\boldsymbol{v}) \qquad (56)
\end{aligned}
$$

Similar with the inequalities (33), (34), (35) and (37), the following inequalities hold:

$$
-\tilde{D}_r\tilde{\boldsymbol{W}}_2^T\boldsymbol{H}_2(\boldsymbol{v}) \le \frac{\mu_2^2}{2}\tilde{D}_r^2 + \frac{1}{2}\tilde{\boldsymbol{W}}_2^T\tilde{\boldsymbol{W}}_2 \qquad (57)
$$

$$
\begin{aligned}
\sigma_2\tilde{\boldsymbol{W}}_2^T\hat{\boldsymbol{W}}_2 &\le -\frac{\sigma_2\tilde{\boldsymbol{W}}_2^T\tilde{\boldsymbol{W}}_2}{4} - \frac{\sigma_2}{4}\left(\tilde{\boldsymbol{W}}_2^T\tilde{\boldsymbol{W}}_2\right)^l\\
&\quad + \frac{\sigma_2\boldsymbol{W}_2^{*T}\boldsymbol{W}_2^*}{2} + \frac{\sigma_2}{4}\Phi_1 \qquad (58)
\end{aligned}
$$

with $\|\boldsymbol{H}_2\| \le \mu_2$, μ_2 is a positive constant.

In addition, defining $z = 1$, $\beta = \tilde{D}_r^2$, $m = 1-l$, $n = l$, $\iota = l^{\frac{l}{1-l}}$, according to Lemma 3, we obtain

$$
-\tilde{D}_r^2 \le -\frac{\tilde{D}_r^2}{2} - \frac{\tilde{D}_r^{2l}}{2} + \frac{(1-l)\,\iota}{2} \qquad (59)
$$

Based on the inequalities (57), (58) and (59), we can rewrite (56) as

$$
\begin{aligned}
V_4 &\le -k_7 r_e^2 - k_8|r_e|^{2l} - \left(\frac{\sigma_2}{4} - \frac{1}{2}\right)\tilde{\boldsymbol{W}}_2^T\tilde{\boldsymbol{W}}_2\\
&\quad - \frac{\sigma_2}{4}\left(\tilde{\boldsymbol{W}}_2^T\tilde{\boldsymbol{W}}_2\right)^l - \left(\frac{p_2}{2} - \frac{1}{4} - \frac{\mu_2^2}{4}\right)\tilde{D}_r^2\\
&\quad - \left(\frac{p_2}{2} - \frac{1}{4} - \frac{\mu_2^2}{4}\right)\tilde{D}_r^{2l} - r_e\psi_e\\
&\quad + (1-l)\left(\frac{p_2}{2} - \frac{1}{4} - \frac{\mu_2^2}{4}\right)\iota + \frac{\sigma_2}{4}\Phi_1\\
&\quad + \frac{\sigma_2\boldsymbol{W}_2^{*T}\boldsymbol{W}_2^*}{2} + \frac{\bar{D}_r^2}{2} \qquad (60)
\end{aligned}
$$

C. STABILITY ANALYSIS

Based on the above formulations, the following theorem is presented to illustrate that under the proposed controller, the tracking errors can converge to a small neighborhood around zero within finite time, while the prescribed position error constraint can never be violated.

Theorem 1: Consider the underactuated MSV system (6), if the initial conditions satisfy that $\rho_e(0) \in \Omega_e = \{\rho_e : |\rho_e(0)| < k_e\}$, and the adaptive laws of the RBFNN weight vector are chosen as (29) and (53), the disturbance observers are given by (30) and (55), the virtual control laws are obtained from (16) and (42), the controllers are designed as (28) and (52) under Assumptions 1-3, then the resulting closed-loop system has the following properties:

(i) The tracking errors of the vessel control system can converge to arbitrarily small neighborhoods around the origin within finite time T_0.

(ii) The position error constraint $|\rho_e| < k_e$ is not violated for all $t \ge 0$.

(iii) All signals in closed-loop system are bounded.

Proof: Construct the complete Lyapunov function as follows

$$
V = V_1 + V_2 + V_3 + V_4 \qquad (61)
$$

With the help of equations (21), (38), (45), (60), the inequality $\log\frac{k_e^2}{k_e^2-\rho_e^2} < \frac{\rho_e^2}{k_e^2-\rho_e^2}$ and Lemma 2, the time derivative of (61) satisfies

$$
\begin{aligned}
\dot{V} &\le -k_1\frac{\rho_e^2}{k_e^2-\rho_e^2} - k_2\frac{\rho_e^{2l}}{\left(k_e^2-\rho_e^2\right)^l} - (k_{c1}-1)\,e_1^2\\
&\quad - k_{c2}|e_1|^{2l} - k_3 u_e^2 - k_4|u_e|^{2l} - \left(\frac{\sigma_1}{4} - \frac{1}{2}\right)\tilde{\boldsymbol{W}}_1^T\tilde{\boldsymbol{W}}_1\\
&\quad - \frac{\sigma_1}{4}\left(\tilde{\boldsymbol{W}}_1^T\tilde{\boldsymbol{W}}_1\right)^l - \left(\frac{p_1}{2} - \frac{\mu_1^2}{4} - \frac{1}{4}\right)\tilde{D}_u^2\\
&\quad - \left(\frac{p_1}{2} - \frac{\mu_1^2}{4} - \frac{1}{4}\right)\tilde{D}_u^{2l} - k_5\psi_e^2 - k_6|\psi_e|^{2l}\\
&\quad - (k_{c3}-1)\,e_2^2 - k_{c4}|e_2|^{2l} - k_7 r_e^2 - k_8|r_e|^{2l}\\
&\quad - \left(\frac{\sigma_2}{4} - \frac{1}{2}\right)\tilde{\boldsymbol{W}}_2^T\tilde{\boldsymbol{W}}_2 - \frac{\sigma_2}{4}\left(\tilde{\boldsymbol{W}}_2^T\tilde{\boldsymbol{W}}_2\right)^l\\
&\quad - \left(\frac{p_2}{2} - \frac{\mu_2^2}{4} - \frac{1}{4}\right)\tilde{D}_r^2 - \left(\frac{p_2}{2} - \frac{\mu_2^2}{4} - \frac{1}{4}\right)\tilde{D}_r^{2l}\\
&\quad + \frac{\sigma_1\boldsymbol{W}_1^{*T}\boldsymbol{W}_1^*}{2} + \frac{\sigma_2\boldsymbol{W}_2^{*T}\boldsymbol{W}_2^*}{2} + \frac{\sigma_1+\sigma_2}{4}\Phi_1\\
&\quad + \frac{\bar{D}_u^2 + \bar{D}_r^2}{2} + (1-l)\left(\frac{p_1+p_2}{2} - \frac{\mu_1^2+\mu_2^2}{4} - \frac{1}{2}\right)\iota\\
&\le -k_{V0}V - k_{V1}V^l + \Delta \qquad (62)
\end{aligned}
$$

with

$$
\frac{p_1}{2} - \frac{\mu_1^2}{4} - \frac{1}{4} > 0,\ \frac{p_2}{2} - \frac{\mu_2^2}{4} - \frac{1}{4} > 0
$$

and

$$
k_{V0} = \min\left\{\begin{matrix} k_1, k_{c1}-1, k_3, \frac{\sigma_1}{4}-\frac{1}{2}, \frac{p_1}{2}-\frac{\mu_1^2}{4}-\frac{1}{4}, k_5, \\ k_{c3}-1, k_7, \frac{\sigma_2}{4}-\frac{1}{2}, \frac{p_2}{2}-\frac{\mu_2^2}{4}-\frac{1}{4} \end{matrix}\right\},
$$

$$
k_{V1} = \min\left\{\begin{matrix} k_2, k_{c2}, k_4, \frac{\sigma_1}{4}, \frac{p_1}{2}-\frac{\mu_1^2}{4}-\frac{1}{4}, \\ k_6, k_{c4}, k_8, \frac{\sigma_2}{4}, \frac{p_2}{2}-\frac{\mu_2^2}{4}-\frac{1}{4}, \end{matrix}\right\},
$$

$$
\begin{aligned}
\Delta &= \frac{\sigma_1\boldsymbol{W}_1^{*T}\boldsymbol{W}_1^*}{2} + \frac{\sigma_2\boldsymbol{W}_2^{*T}\boldsymbol{W}_2^*}{2} + \frac{\sigma_1+\sigma_2}{4}\Phi_1\\
&\quad + (1-l)\left(\frac{p_1+p_2}{2} - \frac{\mu_1^2+\mu_2^2}{4} - \frac{1}{2}\right)\iota\\
&\quad + \frac{\bar{D}_u^2 + \bar{D}_r^2}{2}.
\end{aligned}
$$

(i) From (62), we have

$$
\dot{V} \le -(1-\varsigma)\,k_{V0}V - \varsigma k_{V0}V - k_{V1}V^l + \Delta \qquad (63)
$$

where ς is a positive constant satisfying $0 < \varsigma < 1$. When $V \geq \frac{\Delta}{\varsigma k_{V0}}$, we have $\dot{V} \leq -(1-\varsigma) k_{V0} V - k_{V1} V^l$. Thus, it can be concluded that V will converge to the set $\Omega_V = \left\{V : V < \frac{\Delta}{\varsigma k_{V0}}\right\}$ within finite time, and the settling time T_0 can be estimated as follows based on Lemma 1:

$$T_0 \leq \frac{1}{(1-\varsigma) k_{V0} (1-l)} \ln \frac{(1-\varsigma) k_{V0} V^{1-l}(0) + k_{V1}}{k_{V1}} \tag{64}$$

Furthermore, for $t > T_0$, we have $\frac{1}{2} \log \frac{k_e^2}{k_e^2 - \rho_e^2} \leq V < \frac{\Delta}{\varsigma k_{V0}}$, thus the tracking error ρ_e satisfy the condition $|\rho_e| < k_e \sqrt{1 - e^{-2\Delta/\varsigma k_{V0}}}$ in finite time. Similarly, the other tracking errors included in V will also remain in the small neighborhoods around the origin within finite time.

(ii) Based on (62), we have $\dot{V} \leq -k_{V0} V + \Delta$. Therefore, for $t \geq 0$, the following inequality holds:

$$V(t) \leq \varpi(t) = \left(V(0) - \frac{\Delta}{k_{V0}}\right) e^{-k_{V0} t} + \frac{\Delta}{k_{V0}} \tag{65}$$

According to $V_\rho \leq V$, we can obtain

$$|\rho_e| \leq k_e \sqrt{1 - e^{-2\varpi t}} < k_e \tag{66}$$

Consequently, the prescribed constraint on position tracking error ρ_e can be guaranteed for all $t \geq 0$.

(iii) From the boundedness of V and Assumtion 1, we know $\boldsymbol{\eta}$, e_1, e_2 are bounded. Thus, we can derive $\alpha_{u,c}$ and $\alpha_{r,c}$ are bounded. Since the tracking errors u_e, r_e are bounded, the states u and r are bounded either. Based on Assumption 3, the sway velocity v is also bounded. Therefore, all signals in the closed-loop system are bounded.

Remark 3: Compared with the previous works [10], [17] in which the tracking control laws can only guarantee the asymptotic convergence for an underactuated vessel. However, the tracking errors under our proposed controller have been proved to converge to arbitrarily small neighborhoods around the origin in finite time, which can obtain faster transient response and improved robustness than that of the controllers in [10] and [17].

Remark 4: To compensate for the lumped disturbances, the disturbance observers are designed in (30) and (54). Since the unknown hydrodynamic damping terms are approximated by using RBFNN, and the neural approximation errors are estimated by the designed disturbance observer in real time, our proposed control scheme can obtain more accurate tracking performance as compared to the conventional NN-based control. In addition, our proposed control scheme can estimate the general form of unknown nonlinear dynamics as compared to the control schemes in [33] and [34].

IV. SIMULATIONS

In this section, the simulation studies for an underactuated marine surface vessel are performed to verify the effectiveness of the proposed control scheme. The nominal vessel parameters are adopted from [3], which are listed in Table 1. The comparative control schemes are assigned as follows:

TABLE 1. Nominal values of the marine surface vessel.

Parameter	Value	Unit	Parameter	Value	Unit
m_{11}	1.1274	kg	d_v	0.1183	kg/s
m_{22}	1.8902	kg	d_{v2}	0.05915	kg/m
m_{33}	0.1278	kgm^2	d_{v3}	0.029575	kgs/m^2
d_u	0.0358	kg/s	d_r	0.0308	kgm^2/s
d_{u2}	0.0179	kg/m	d_{r2}	0.0154	kgm^2
d_{u3}	0.00895	kgs/m^2	d_{r3}	0.0077	$kgm^2 s$

(i) Asymptotically tracking control (ATC): This comparative controller is obtained from [17], in which the tracking errors of an underactuated vessel asymptotically converge to a small neighborhood of the origin; (ii) Adaptive neural-based finite-time tracking control (ANFTC): The control scheme in this case is our designed controller (28) and (52). The position error constraint is selected as $k_e = 1.5\ m$. The control parameters are set as: $k_1 = 0.5$, $k_2 = 0.5$, $k_3 = 4$, $k_4 = 1.7$, $k_5 = 5$, $k_6 = 1$, $k_7 = 0.2$, $k_8 = 1.7$, $k_m = 2$, $k_n = 1.5$, $p_1 = 1.5$, $p_2 = 2.55$, $\sigma_1 = 2.55$, $\sigma_2 = 2.05$. Since RBFNN is used to approximate the unknown terms $f_u(u)$ and $f_r(r)$, the NN input for $\boldsymbol{H}_1(\boldsymbol{\nu})$ is chosen as $\boldsymbol{\nu} = \left[u, u^2, u^3\right]^T$, and the NN input for $\boldsymbol{H}_2(\boldsymbol{\nu})$ is $\boldsymbol{\nu} = \left[r, r^2, r^3\right]^T$. The hidden node numbers for $\hat{\boldsymbol{W}}_1^T \boldsymbol{H}_1(\boldsymbol{\nu})$ and $\hat{\boldsymbol{W}}_2^T \boldsymbol{H}_2(\boldsymbol{\nu})$ are set to $n = 13$, with centers $\boldsymbol{\phi}_{l_1}$ $(l_1 = 1, \cdots, n)$ and $\boldsymbol{\phi}_{l_2}$ $(l_2 = 1, \cdots, n)$ evenly spaced in $[0, 5]$ and $[-0.2, 0.2]$, respectively. The widths are selected as $\delta_{l_1} = 5$ and $\delta_{l_2} = 1$, respectively.

A. CIRCULAR TRACKING SIMULATION

In this case, the desired trajectory is generated by the virtual vessel (8), $u_d = 1.5$ m/s, $v_d = 0$ m/s, $r_d = 3$ deg/s. It should be noted that the desired velocities should be chosen properly in order to avoid the effects of the actuators saturation. The initial conditions are chosen as: $\boldsymbol{\eta}(0) = [-1\ m, -1\ m, 0.45\ rad]^T$, $\boldsymbol{\nu}(0) = [0\ m/s, 0\ m/s, 0\ rad/s]^T$, $\boldsymbol{\eta}_d(0) = [0\ m, 0\ m, 0\ rad]^T$. It can be seen that $\rho_e(0) = \sqrt{2} < k_e = 1.5$. The external disturbances are assumed to be

$$\begin{bmatrix} \tau_{wu}(t) \\ \tau_{wv}(t) \\ \tau_{wr}(t) \end{bmatrix} = \begin{bmatrix} 0.2\,(1 + 3\sin(0.2t + \pi/2)) \\ 0.1\,(1 + 1.5\cos(0.1t + \pi/6)) \\ 0.25\,(0.8 + 2\cos(0.15t - \pi/5)) \end{bmatrix}$$

The comparative simulation results of our designed ANFTC method and the ATC method in [17] are shown in Figs. 4-11. The circular trajectory tracking is shown in Fig. 4. It can be seen that the proposed controller has improved tracking performance in terms of convergence rate. Fig. 5 shows the position tracking errors with respect to EF, which illustrates that the ANFTC method can achieve faster error stabilization as compared to the ATC method. The total position tracking error ρ_e and the heading tracking error ψ_e are presented in Fig. 6, from the partial enlarged view we can see that the tracking errors under our proposed controller can converge to a small neighborhood around the origin quickly and keep the stable state thereafter. However, there exists larger steady-state tracking errors by using the

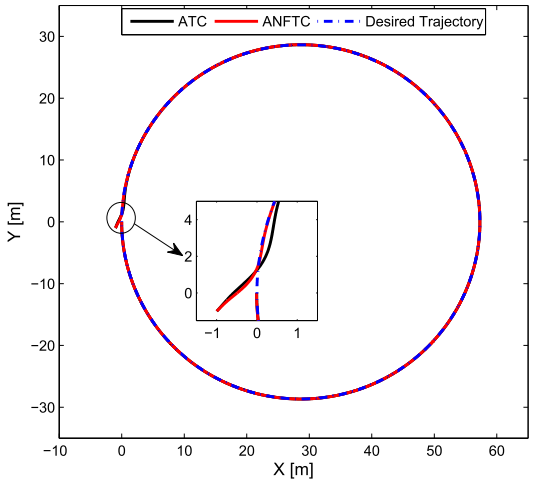

FIGURE 4. Trajectory of circular tracking.

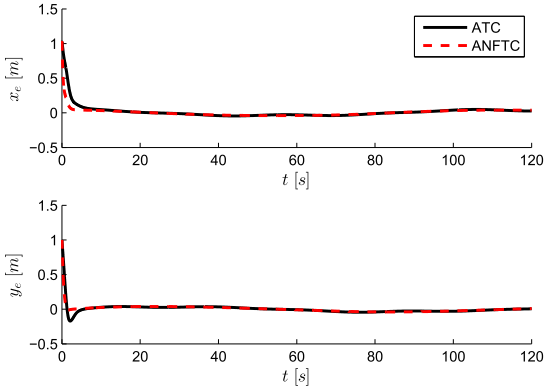

FIGURE 5. Position errors of circular tracking.

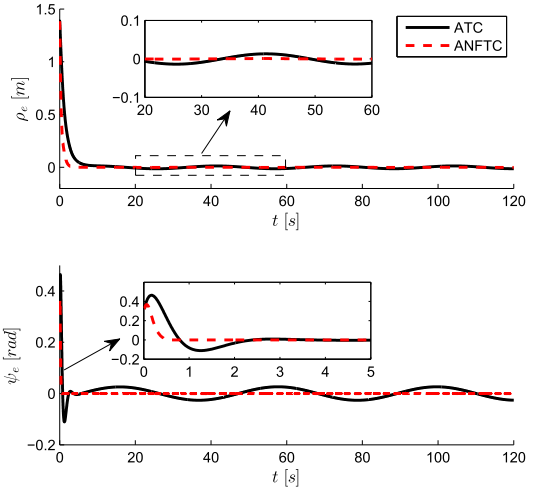

FIGURE 6. Position and attitude errors of circular tracking.

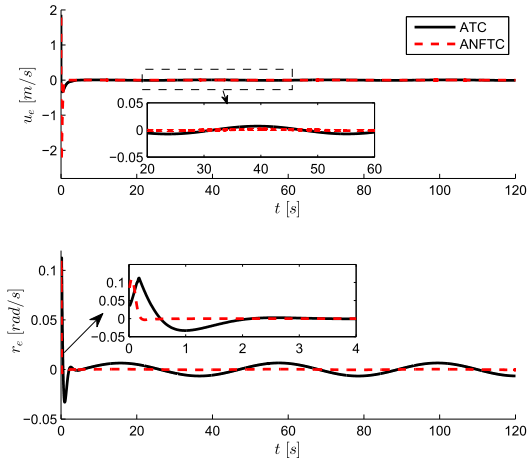

FIGURE 7. Velocity errors of circular tracking.

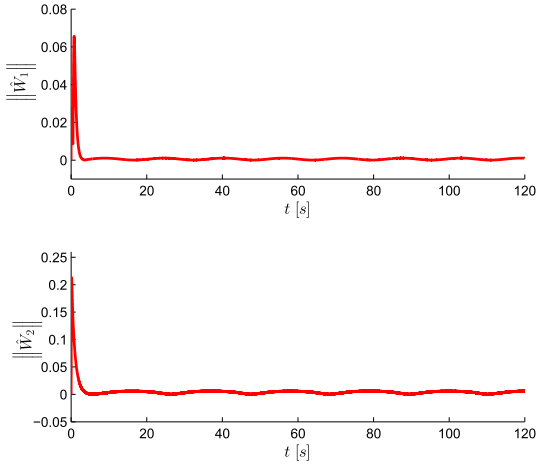

FIGURE 8. Norms of RBFNN weights under the proposed control scheme.

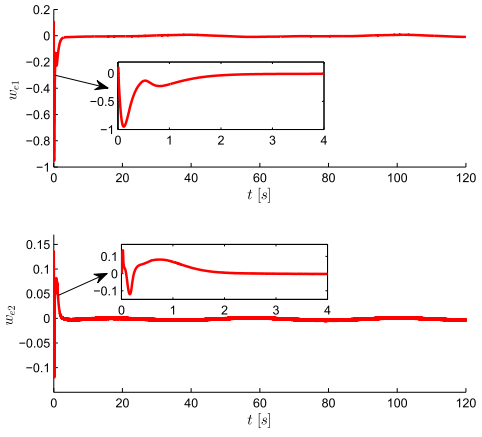

FIGURE 9. Time response of RBFNN approximation errors.

ATC method. In addition, the predefined position error constraint is never overstepped. Fig. 7 compares the velocity tracking results under these two different control schemes, it can be seen that the proposed controller has faster convergence speed and higher tracking accuracy than that of the ATC method. The norms of the adaptive law for RBFNN weight are shown in Fig. 8. The RBFNN approximation errors $w_{e1} = p_1^{-1}\hat{\boldsymbol{W}}_1^T\boldsymbol{H}_1(\boldsymbol{v}) - f_u(u)$ and $w_{e2} = p_2^{-1}\hat{\boldsymbol{W}}_2^T\boldsymbol{H}_2(\boldsymbol{v}) -$

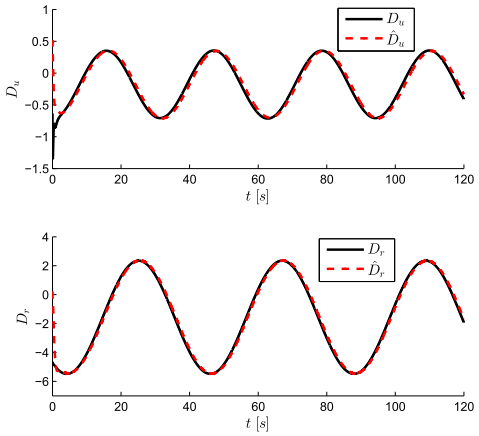

FIGURE 10. Disturbances and their estimated values.

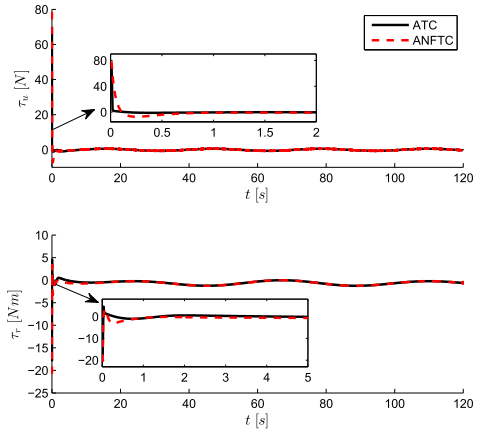

FIGURE 11. Control inputs of circular tracking.

$f_r(r)$ are illustrated in Fig. 9. The compound disturbances $D_u(t), D_r(t)$ and their estimated values are shown in Fig. 10, respectively. It is shown that the designed disturbance observer can provide good estimation performance. The control inputs under these two controllers are shown in Fig. 11. It can be seen that the initial control inputs under the proposed controller are slightly larger than that under the ATC method. This is because the proposed control scheme is required to drive the vessel to the desired trajectory with shorter time.

B. GENERAL CURVILINEAR TRACKING SIMULATION

To further verify the tracking performance of the proposed control scheme, a general curvilinear trajectory tracking simulation is provided in this subsection. The desired trajectory is composed with a straight line and a circular arc. The reference trajectory is generated by choosing $u_d = 1.2$ m/s, $v_d = 0$ m/s, and $r_d = 0$ deg/s for $0\,s \le t < 50\,s$, $r_d = 2.5$ deg/s for $50\,s \le t \le 120\,s$. The initial conditions are set as $\boldsymbol{\eta}(0) = [1\,m, -1\,m, 1.3\,rad]^T$, $\boldsymbol{\nu}(0) = [0\,m/s, 0\,m/s, 0\,rad/s]^T$, $\boldsymbol{\eta}_d(0) = [0\,m, 0\,m, \pi/2\,rad]^T$. The initial position error satisfies that $\rho_e(0) < k_e$. The external disturbances are

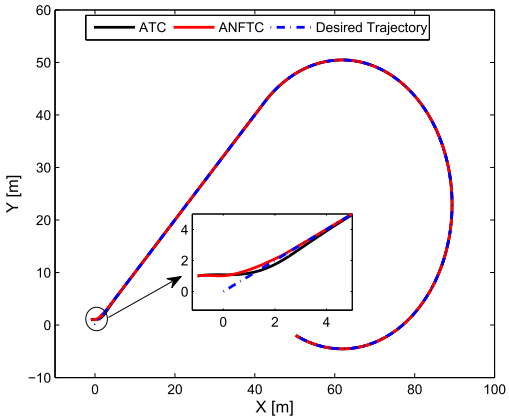

FIGURE 12. Trajectory of general curvilinear tracking.

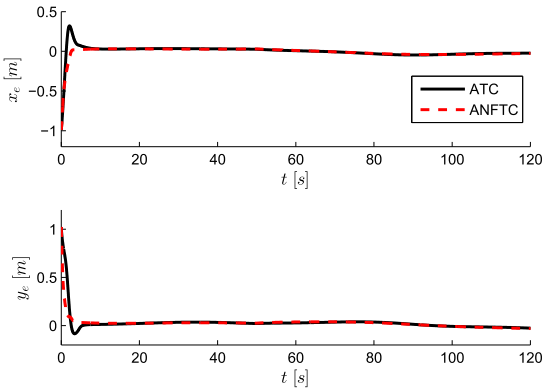

FIGURE 13. Position errors of general curvilinear tracking.

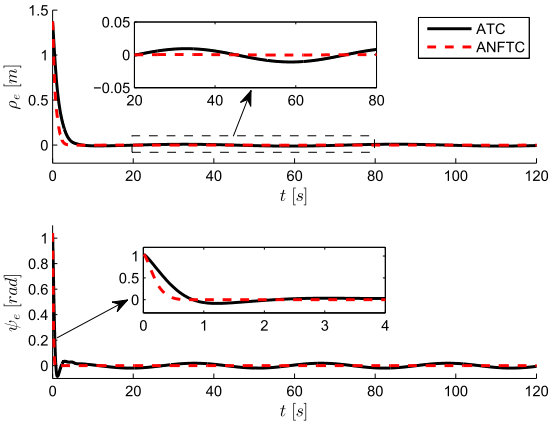

FIGURE 14. Position and attitude errors of general curvilinear tracking.

selected as

$$\begin{bmatrix} \tau_{wu}(t) \\ \tau_{wv}(t) \\ \tau_{wr}(t) \end{bmatrix} = \begin{bmatrix} 0.3\,(1.2 + 2.5\sin(0.12t - \pi/6)) \\ 0.1\,(1 + 1\cos(0.1t + \pi/4)) \\ 0.2\,(1 + 1.5\cos(0.2t + \pi/3)) \end{bmatrix}$$

The simulation results under our proposed controller and the controller in [17] are presented in Figs. 12-19. Fig. 12 shows the time history of vessel position under these two control schemes. It can be observed that the proposed

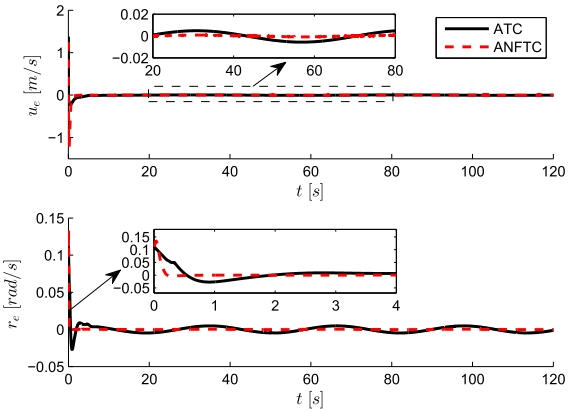

FIGURE 15. Velocity errors of general curvilinear tracking.

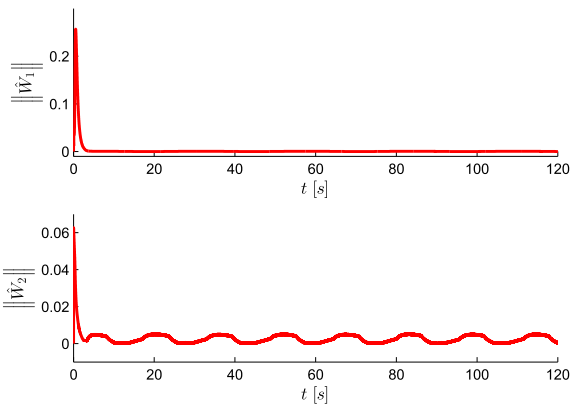

FIGURE 16. Norms of RBFNN weights under the proposed control scheme.

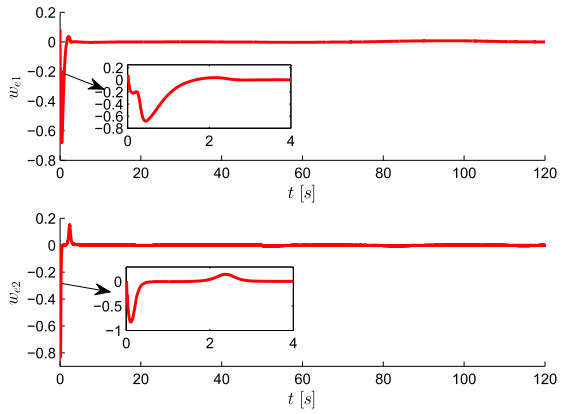

FIGURE 17. Time response of RBFNN approximation errors.

ANFTC method has faster convergence speed compared with the ATC method. The position and heading tracking errors are illustrated in Fig. 13 and Fig. 14, respectively, which demonstrate that the proposed controller has faster transient response and higher tracking precision as compared to the ATC method. Moreover, the position tracking error ρ_e can always remain in the prescribed constraint. The velocity tracking results are plotted in Fig. 15. We can

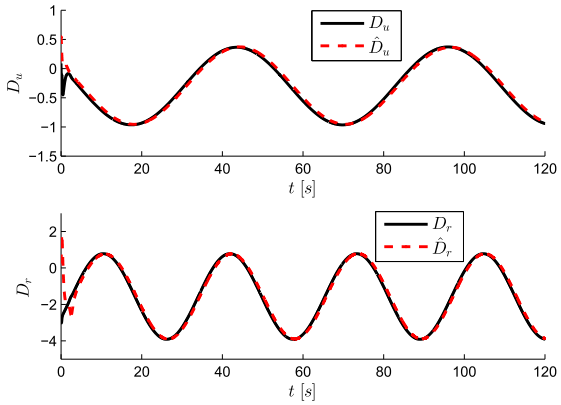

FIGURE 18. Disturbances and their estimated values.

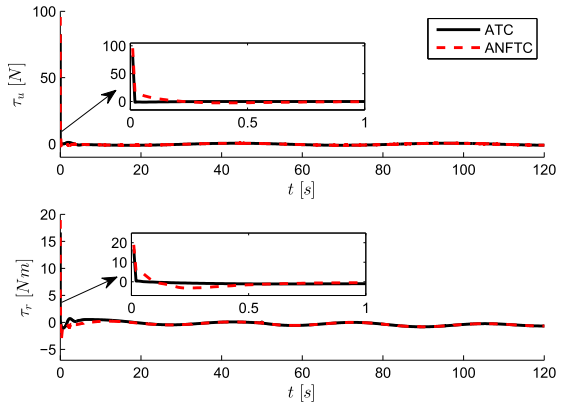

FIGURE 19. Control inputs of general curvilinear tracking.

see that the velocity errors under the proposed control method can converge to near zero and remain stable with faster speed. The response curves of the adaptive laws for RBFNN weight $\|\hat{W}_1\|$ and $\|\hat{W}_2\|$ are shown in Fig. 16. The RBFNN approximation errors are illustrated in Fig. 17. The lumped disturbances and the corresponding estimation values are shown in Fig. 18. We can see that the proposed disturbance observer can provide a good disturbance estimation. Fig. 19 presents the control inputs under these two comparative controllers. It should be noted that the amplitude of the initial input signal under the ANFTC method is larger than that of the ATC method, which allows the vessel to track the desired trajectory more quickly at the beginning.

V. CONCLUSION

A finite-time trajectory tracking control scheme for an underactuated marine surface vessel with position error constraint and system uncertainties has been proposed in this paper. The tracking errors of the MSV control system have been regulated to a small neighborhood around the origin within finite time by resorting to disturbance observer-based finite time control and RBFNN theory. Furthermore, The position tracking error has been constrained to a prescribed region for all time by introducing a BLF into the adaptive backstepping procedure. The command filters and auxiliary systems are

adopted to reduce the complexity of the designed controller. The unknown items are estimated by using adaptive RBFNN and the disturbance rejection ability has been verified by using the designed disturbance observer. Simulation results have shown that the proposed control algorithm has improved control performance with respect to convergence rate and tracking accuracy. Future work will address the actuators saturation problem of tracking control for underactuated MSVs.

REFERENCES

[1] M. Reyhanoglu, "Exponential stabilization of an underactuated autonomous surface vessel," *Automatica*, vol. 33, no. 12, pp. 2249–2254, Dec. 1997.

[2] Z. Sun, G. Zhang, L. Qiao, and W. Zhang, "Robust adaptive trajectory tracking control of underactuated surface vessel in fields of marine practice," *J. Mar. Sci. Technol.*, vol. 23, no. 4, pp. 950–957, Dec. 2018.

[3] J. Ghommam, S. El Ferik, and M. Saad, "Robust adaptive path-following control of underactuated marine vessel with off-track error constraint," *Int. J. Syst. Sci.*, vol. 49, no. 7, pp. 1540–1558, Mar. 2018.

[4] T. I. Fossen, *Handbook of Marine Craft Hydrodynamics and Motion Control*. New York, NY, USA: Wiley, 2011.

[5] Z.-P. Jiang, "Global tracking control of underactuated ships by Lyapunov's direct method," *Automatica*, vol. 38, no. 2, pp. 301–309, Feb. 2002.

[6] K. D. Do and J. Pan, "Global tracking control of underactuated ships with nonzero off-diagonal terms in their system matrices," *Automatica*, vol. 41, no. 1, pp. 87–95, Jan. 2005.

[7] R. Yu, Q. Zhu, G. Xia, and Z. Liu, "Sliding mode tracking control of an underactuated surface vessel," *IET Control Theory Appl.*, vol. 6, no. 3, pp. 461–466, Feb. 2012.

[8] T. Elmokadem, M. Zribi, and K. Youcef-Toumi, "Trajectory tracking sliding mode control of underactuated AUVs," *Nonlinear Dyn.*, vol. 84, no. 2, pp. 1079–1091, Apr. 2016.

[9] C. Liu, Z. Zou, and J. Yin, "Trajectory tracking of underactuated surface vessels based on neural network and hierarchical sliding mode," *J. Mar. Sci. Technol.*, vol. 20, no. 2, pp. 322–330, Jun. 2015.

[10] Z. Sun, G. Zhang, B. Yi, and W. Zhang, "Practical proportional integral sliding mode control for underactuated surface ships in the fields of marine practice," *Ocean Eng.*, vol. 142, pp. 217–223, Sep. 2017.

[11] J. Xu, M. Wang, and L. Qiao, "Dynamical sliding mode control for the trajectory tracking of underactuated unmanned underwater vehicles," *Ocean Eng.*, vol. 105, pp. 54–63, Sep. 2015.

[12] W. He, Z. Yin, and C. Sun, "Adaptive neural network control of a marine vessel with constraints using the asymmetric barrier Lyapunov function," *IEEE Trans. Cybern.*, vol. 47, no. 7, pp. 1641–1651, Jul. 2017.

[13] K. Shojaei, "Neural adaptive robust control of underactuated marine surface vehicles with input saturation," *Appl. Ocean Res.*, vol. 53, pp. 267–278, Oct. 2015.

[14] G. Li, W. Li, H. P. Hildre, and H. Zhang, "Online learning control of surface vessels for fine trajectory tracking," *J. Mar. Sci. Technol.*, vol. 21, no. 2, pp. 251–260, Jun. 2016.

[15] L. Kong, W. He, C. Yang, G. Li, and Z. Zhang, "Adaptive fuzzy control for a marine vessel with time-varying constraints," *IET Control Theory Appl.*, vol. 12, no. 10, pp. 1448–1455, Mar. 2018.

[16] N. Wang, M. J. Er, J.-C. Sun, and Y.-C. Liu, "Adaptive robust online constructive fuzzy control of a complex surface vehicle system," *IEEE Trans. Cybern.*, vol. 46, no. 7, pp. 1511–1523, Jul. 2016.

[17] D. D. Mu, G. F. Wang, and Y. S. Fan, "Tracking control of podded propulsion unmanned surface vehicle with unknown dynamics and disturbance under input saturation," *Int. J. Control, Autom. Syst.*, vol. 16, no. 4, pp. 1905–1915, Aug. 2018.

[18] O. Elhaki and K. Shojaei, "Neural network-based target tracking control of underactuated autonomous underwater vehicles with a prescribed performance," *Ocean Eng.*, vol. 167, pp. 239–256, Nov. 2018.

[19] N. Wang and M. J. Er, "Self-constructing adaptive robust fuzzy neural tracking control of surface vehicles with uncertainties and unknown disturbances," *IEEE Trans. Control Syst. Technol.*, vol. 23, no. 3, pp. 991–1002, May 2015.

[20] J. Xia, J. Zhang, W. Sun, B. Zhang, and Z. Wang, "Finite-time adaptive fuzzy control for nonlinear systems with full state constraints," *IEEE Trans. Syst., Man, Cybern., Syst.*, to be published, doi: 10.1109/TSMC.2018.2854770.

[21] S. Zhao, H. Liang, P. Du, and S. Qi, "Adaptive NN finite-time tracking control of output constrained nonlinear system with input saturation," *Nonlinear Dyn.*, vol. 92, no. 4, pp. 1845–1856, Jun. 2018.

[22] O. Mofid and S. Mobayen, "Adaptive sliding mode control for finite-time stability of quad-rotor UAVs with parametric uncertainties," *ISA Trans.*, vol. 72, pp. 1–14, Jan. 2018.

[23] H. Du and S. Li, "Finite-time attitude stabilization for a rigid spacecraft using homogeneous method," in *Proc. 18th IFAC World Congr.*, Milan, Italy, 2011, pp. 2620–2625.

[24] L. Zhao, J. Yu, and H. Yu, "Adaptive finite-time attitude tracking control for spacecraft with disturbances," *IEEE Trans. Aerosp. Electron. Syst.*, vol. 54, no. 3, pp. 1297–1305, Jun. 2018.

[25] N. Wang, S. Lv, W. Zhang, Z. Liu, and M. J. Er, "Finite-time observer based accurate tracking control of a marine vehicle with complex unknowns," *Ocean Eng.*, vol. 145, pp. 406–415, Nov. 2017.

[26] N. Wang, S. Lv, M. J. Er, and W.-H. Chen, "Fast and accurate trajectory tracking control of an autonomous surface vehicle with unmodeled dynamics and disturbances," *IEEE Trans. Intell. Veh.*, vol. 1, no. 3, pp. 230–243, Sep. 2016.

[27] N. Wang, C. Qian, J.-C. Sun, and Y.-C. Liu, "Adaptive robust finite-time trajectory tracking control of fully actuated marine surface vehicles," *IEEE Trans. Control Syst. Technol.*, vol. 24, no. 4, pp. 1454–1462, Jul. 2016.

[28] K. P. Tee, S. S. Ge, and E. H. Tay, "Barrier Lyapunov functions for the control of output-constrained nonlinear systems," *Automatica*, vol. 45, no. 4, pp. 918–927, Apr. 2009.

[29] Y.-J. Liu and S. Tong, "Barrier Lyapunov functions for Nussbaum gain adaptive control of full state constrained nonlinear systems," *Automatica*, vol. 76, pp. 143–152, Feb. 2017.

[30] Z. Zheng, Y. Huang, L. Xie, and B. Zhu, "Adaptive trajectory tracking control of a fully actuated surface vessel with asymmetrically constrained input and output," *IEEE Trans. Control Syst. Technol.*, vol. 26, no. 5, pp. 1851–1859, Sep. 2018.

[31] W. He and T. Ma, "Adaptive neural network control of a vessel with output constraints using the asymmetric barrier Lyapunov function," in *Proc. 3rd IFAC Conf. Intell. Control Automat. Sci. (ICONS)*, Chengdu, China, 2013, pp. 246–251.

[32] X. Jin, "Adaptive finite-time fault-tolerant tracking control for a class of MIMO nonlinear systems with output constraints," *Int. J. Robust Nonlinear Control*, vol. 27, no. 5, pp. 722–741, Mar. 2017.

[33] X. Jin, "Fault tolerant finite-time leader-follower formation control for autonomous surface vessels with LOS range and angle constraints," *Automatica*, vol. 68, pp. 228–236, Jun. 2016.

[34] H. Li, S. Zhao, W. He, and R. Lu, "Adaptive finite-time tracking control of full state constrained nonlinear systems with dead-zone," *Automatica*, vol. 100, pp. 99–107, Feb. 2019.

[35] M. Chen, S. S. Ge, and B. Ren, "Adaptive tracking control of uncertain MIMO nonlinear systems with input constraints," *Automatica*, vol. 47, no. 3, pp. 452–465, Mar. 2011.

[36] M. Chen and S. S. Ge, "Direct adaptive neural control for a class of uncertain nonaffine nonlinear systems based on disturbance observer," *IEEE Trans. Cybern.*, vol. 43, no. 4, pp. 1213–1225, Aug. 2013.

[37] J.-H. Li, P.-M. Lee, B.-H. Jun, and Y.-K. Lim, "Point-to-point navigation of underactuated ships," *Automatica*, vol. 44, no. 12, pp. 3201–3205, Dec. 2008.

[38] S. S. Ge, C. C. Hang, T. H. Lee, and T. Zhang, *Stable Adaptive Neural Network Control*. Boston, MA, USA: Springer, 2002.

MINGYU FU received the Ph.D. degree from the College of Automation, Harbin Engineering University, Harbin, China, in 2005, where she is currently a Professor and a Ph.D. Supervisor. Her current research interests include vessel dynamic positioning control, automatic control of unmanned surface vehicle, and hovercraft motion control.

TAIQI WANG received the B.E. degree in automation from Harbin Engineering University, Harbin, China, in 2014, where he is currently pursuing the Ph.D. degree in control science and engineering with the College of Automation. His main research interests include robust adaptive control and motion control of marine surface vessel.

CHENGLONG WANG received the Ph.D. degree from the College of Automation, Harbin Engineering University, Harbin, China, in 2009, where he is currently an Associate Professor. His current research interests include vessel dynamic positioning control, vessel intelligent control, and artificial intelligence control.